Prepositioned single quantum dot in a lateral electric field

M. E. Reimer,[1,2,*] M. Korkusiński,[1] D. Dalacu,[1] J. Lefebvre,[1] J. Lapointe,[1] P. J. Poole,[1] G. C. Aers,[1] W. R. McKinnon,[1] P. Hawrylak,[1,2] and R. L. Williams

[1]*Institute for Microstructural Sciences, National Research Council of Canada, Ottawa, Ontario, Canada K1A 0R6*

[2]*Department of Physics, University of Ottawa, Ottawa, Ontario, Canada K1N 6N5*

(Received 22 August 2008; revised manuscript received 9 October 2008; published 4 November 2008)

We examine the effect of a lateral electric field on the optical properties of a single deterministically positioned InAs/InP quantum dot. We show experimentally that the ground-state excitonic Stark shift is significantly reduced in comparison with the single-particle picture and that the lateral electric field introduces a new previously forbidden optical transition. Results of full configuration-interaction calculations show that the Coulomb interactions of electrons and holes are modified by the electric field leading to the compensation of the single-particle Stark shift. The calculations also account for the appearance of the field-activated optical transition as an excitonic recombination event. The comparison of exciton and predicted charged exciton spectra allows us to exclude the presence of charged exciton complexes within the measured emission spectra. The ability to precisely position a single quantum dot and demonstrate control over the electronic properties of such a dot is expected to find application in scalable techniques for quantum information science.

DOI: 10.1103/PhysRevB.78.195301 PACS number(s): 78.67.Hc, 73.21.La, 78.55.Cr

I. INTRODUCTION

Semiconductor quantum dots (QDs) are strongly confined systems in which the Coulomb interactions between optically generated electrons and holes, as well as the dot size, shape, and compositional structure, play a major role in determining transition energies and oscillator strengths.[1] If such QDs are to be employed within a fully scalable quantum information processing architecture, a method to deterministically position individual dots and manipulate their properties postgrowth is required. This requirement can be met using a nanotemplate deposition technique,[2] where arrays of individual InAs/InP QDs with known location can be produced. Individual dots can then be embedded within photonic crystal (PC) microcavities[3] or manipulated with electrostatic gates[4,5] to obtain the required level of control over their electronic makeup and coupling to the optical field. The ability to manipulate individual QDs postgrowth offers a fully scalable route to sources of single photons[6–9] and entangled photon pairs[5,10–13] for use within quantum cryptographic and quantum information processing systems. For fiber-based quantum cryptography, InAs/InP QDs are particularly attractive since the ground-state transition can be tuned to the telecommunications wavelength of 1.55 μm.[6,7]

Current proposals for the generation of entangled photon pairs using the biexciton-exciton-vacuum cascade within semiconductor QDs rely on the removal of the fine-structure splitting of the intermediate exciton states.[11–16] To date, removal of this anisotropic exchange splitting (AES) for the exciton has been demonstrated only within randomly located QDs through the application of external magnetic fields,[11] spectral filtering,[12] quantum-dot size and composition engineering,[13] or application of in-plane electric fields,[14–16] while the application of a vertical electric field was used to control the charge[17] and field-induced Stark shift of QD states.[18,19]

For methods based on the application of an in-plane electric field, however, the oscillator strength of the transitions is significantly reduced at the electric field required to remove the AES. For scalability, one would like to generate entangled pairs of photons from deterministically positioned arrays of single QDs, utilizing a scheme that does not necessitate the removal of the fine-structure splitting, as proposed elsewhere.[5,10] With this view in mind, we investigate here the optical emission of excitonic complexes within single deterministically positioned InAs/InP QDs subject to an in-plane electric field, where control over the dot nucleation site allows one to precisely position the electrostatic gates with respect to the dot. Previous work in this area[14–16,20,21] used randomly nucleated QDs.

In this work, we first present experimental optical data from a single prepositioned QD as a function of the applied lateral field. We find that in addition to the expected reduction in the fine-structure splitting under applied lateral field, as observed in a previous work on randomly nucleated QDs,[14–16,20] we observe a strong compensation of the ground-state excitonic Stark shift and a new optically allowed transition that appears under applied bias. We show that these effects do not occur if the field is applied along the growth direction. Next, we model our system theoretically using the effective-mass approach coupled with a configuration-interaction (CI) treatment of the states of the electron-hole (eh) pair. In this approach, the suppression of the Stark shift is accounted for by the reduction in the Coulomb interactions among carriers. Further, the additional maximum is identified as a radiative recombination of the neutral exciton in an excited state rather than a signature of charged excitons.

This paper is organized as follows. In Sec. II we present experimental optical data from two different devices containing a single prepositioned QD as a function of applied lateral field (labeled as QD1 and QD2, respectively). In Sec. III we present the theoretical model that describes the effects of the applied electric field. The experimentally observed compensation of the Stark shift is discussed in Sec. III A, and the observation of a field-activated optical transition is presented in Sec. III B. In Sec. IV we discuss the absence of charged

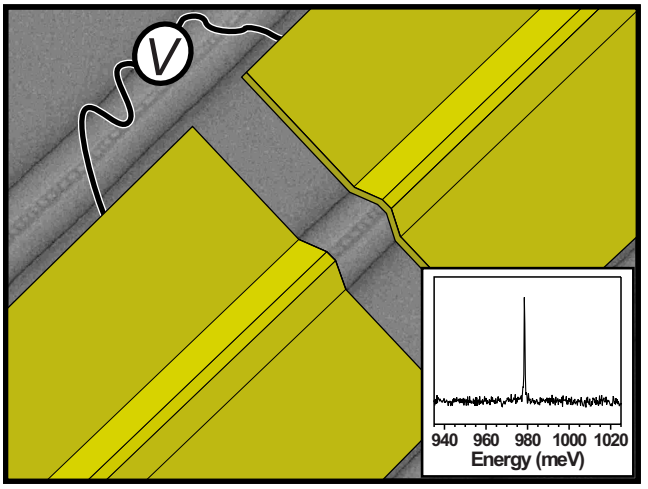

FIG. 1. (Color online) Schematic view of the device showing two metallic gates on top of a scanning electron microscope (SEM) micrograph of an uncapped stripe geometry InP ridge. A linear array of InAs QDs is seen at the apex of the ridge, in the gap (300 nm) separating the gates. In real devices, the QDs are capped with InP prior to gate deposition, and the dot density is chosen to be lower than that shown here so that individual dots can be isolated. Shown in the inset is a typical photoluminescence (PL) spectrum at 4.2 K with a power of approximately 0.01 W/cm^2. The emission line at 978.5 meV is resolution limited (~0.25 meV).

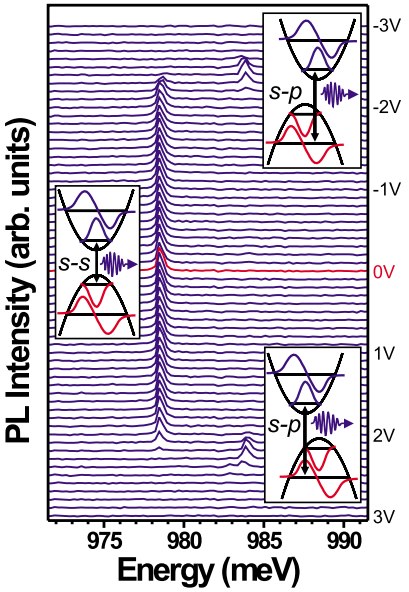

FIG. 2. (Color online) Typical photoluminescence spectra as a function of the lateral electric field at T=4.2 K for both bias directions. A schematic view of the allowed transition (s-s) at 0 V and forbidden transition (s-p_x) at ±2.2 V are shown in the inset. The electron wave functions are shown in blue, and hole wave functions are shown in red.

exciton emission within our data, and in Sec. V we present the summary and conclusions.

II. EXPERIMENT

Figure 1 shows a schematic view of the sample used in the present experiments. InAs dots are nucleated at the apex of a "stripe geometry" InP nanotemplate and subsequently capped with InP. These templates, produced *in situ* during crystal growth, allow one to control the surface migration of deposited InAs so that the nucleation site of the dots can be selected *a priori*.[2] Pairs of metallic Schottky gates deposited across the InP nanotemplate, with narrow (300 nm) gaps, allow in-plane electric fields to be applied along the stripe (x-) direction and serve to isolate the luminescence from individual QDs if the dot density is made sufficiently low. The inset of Fig. 1 shows typical photoluminescence data from such a structure, demonstrating that we have indeed isolated a single QD (QD1). From the power dependence of the emission, we identify the peak at 978.5 meV as the radiative recombination of the neutral exciton (X) ground state, involving a single electron-hole pair from the quantum-dot s-shell. Our assignment is corroborated by the observation of an anisotropic exchange splitting in the ground-state transitions from some dots,[5] as will be discussed in Sec. II B. The p-shell transitions for QD1 presented in Fig. 1 begin around 990 meV (Ref. 4). Experimental and theoretical investigations of single InAs quantum dots nucleated on InP nanotemplates[22,23] show that the nanotemplate controlling the nucleation site of the QD does not degrade its optical quality. The experiments discussed here were performed at 4.2 K using nonresonant above band gap excitation, with detection of the emitted photons achieved using a cooled InGaAs diode array after spectral dispersion in a single grating spectrometer.

A. Application of a lateral electric field

Single-dot photoluminescence under applied lateral field is shown for QD1 in the main panel of Fig. 2, which is typical for such a deterministically positioned QD. For these electric-field measurements, the incident pump intensity was chosen to excite only the ground-state transition from the QD at zero applied electric field. At 0 V bias, only the single X emission line at 978.5 meV is observed. The X transition is seen to retain its oscillator strength under applied field until biases of approximately ±2.0 V, at which point it quickly quenches. As the X transition loses oscillator strength, a second transition appears at approximately 5 meV higher energy, which is itself quenched at higher bias. A schematic of our interpretation of the effects of the applied lateral electric field, to be discussed theoretically in more detail in Sec. III, is shown in the inset of Fig. 2. Here, the addition of a linearly varying potential has the effect of misaligning the centers of the electron and hole parabolic confining potentials and of reducing the energy gap, i.e., producing a Stark shift. At 0 V bias, the wave-function overlap for s-shell electrons and s-shell holes is maximal, as shown in the central inset of Fig. 2. With increasing lateral field, this wave-function overlap decreases as the electron and hole are separated, while the excited-state overlap, corresponding to an s-shell electron and p-shell hole, increases (top and bottom insets of Fig. 2). This newly allowed transition, an s-shell electron recombining with a p-shell hole, is associated with the transition ob-

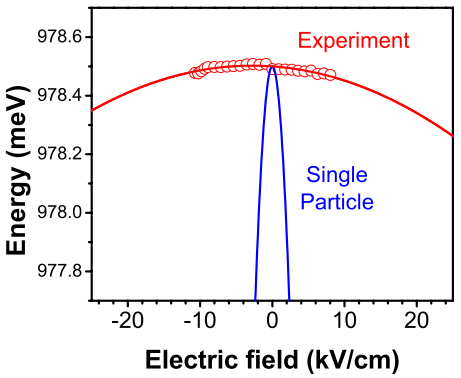

FIG. 3. (Color online) Comparison of calculated single-particle Stark shift (solid blue line) and measured Stark shift (open circles) for the single exciton ground state, *X*, in an applied lateral electric field. The solid red line is a quadratic fit to the measured data.

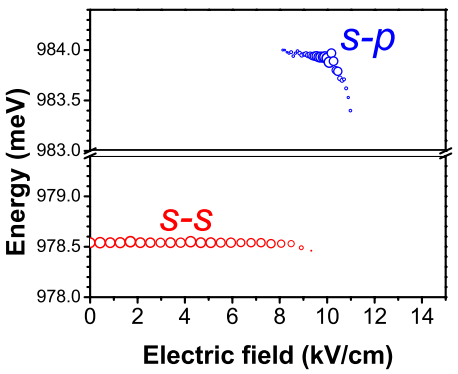

FIG. 4. (Color online) Measured emission maxima for the *s-p* transition appearing under applied bias (open blue circles) and for the *s-s* ground-state transition (open red circles). The size of the symbols represents the normalized integrated intensity.

served at 984 meV in Fig. 2. Since the measured Stark shift of the ground state *X* in Fig. 2 is surprisingly small and not immediately apparent within the spectral resolution, the additional maximum is used to confirm the application of a lateral electric field.

In Fig. 3 we show the peak positions of *X* as a function of the lateral electric field for both bias directions (open circles) at higher spectral resolution. The experimental data are compared with estimates computed using confinement energies typical of InAs/InP QDs (solid blue line). In these estimates we account for single-particle Stark shifts of the electron and hole energies but neglect the Coulomb interactions (see Sec. III). Data are given for an electric-field range of ± 10 kV/cm, in which the *X* transition retains its finite oscillator strength. The electric field is calibrated using the fitting procedure discussed in Sec. III B, which allows us to conclude that electric-field screening effects are minimal for the data presented here. From a quadratic fit of the data (Fig. 3—solid red line) we obtain a polarizability of $\beta=0.31$ μeV cm^2/kV^2, i.e., more than two orders of magnitude smaller than the value of $\beta=144$ μeV cm^2/kV^2 that is estimated theoretically. Note that the single-particle estimates for the polarizability in *vertical* fields are $\beta=2.1$ μeV cm^2/kV^2 for InAs/InP QDs and $\beta=0.81$ μeV cm^2/kV^2 for InGaAs/GaAs QDs. These estimates are only slightly larger than the measured values of $\beta=1.7$ μeV cm^2/kV^2 for a single InAs/InP QD and $\beta=0.66$ μeV cm^2/kV^2 for a single InGaAs/GaAs QD.[24]

In Fig. 4 we show the energy of the *s-p* transition peak from Fig. 2 as a function of positive lateral electric field (identical behavior is found for the opposite field direction). The polarizability of the *s-p* transition is found to be 108 μeV cm^2/kV^2, i.e., two orders of magnitude larger than the experimentally observed polarizability of the *s-s* transition. This allows us to exclude an interpretation for the new field-induced transition as a charged exciton feature, since we expect the Stark shift of charged excitons to be similar to that of the *s-s* neutral exciton (see Sec. IV).

Finally, we comment on the symmetric nature of the optical response observed in Fig. 2. The insensitivity of the data to electric-field direction is expected within the present interpretation but is unlikely if the peak appearing under applied bias is a result of additional charges being added to the system.[25] This is because the existence of any charge traps would be expected to break the symmetry of the system. However, such a symmetric behavior is not observed in all cases since some of the Schottky gates are leaky in one direction. From the symmetric behavior of the ground state *X*, we determine a static dipole for the exciton of $p=3.2\times10^{-30}$ C m. This corresponds to a zero-field electron-hole separation of $\sim$0.02 nm in the lateral direction. This is to be compared with a zero-field electron-hole separation of $\sim$0.5 nm for single InGaAs/GaAs QDs subjected to vertical electric fields.[24] The small static dipole suggests near reflection symmetry for the in-plane direction of our QD.

The behavior, illustrated in Fig. 2, is typical of single InAs quantum dots nucleated on stripe geometry templates and has been observed on eight separate QDs, which are nucleated on templates with a variety of widths. Over the eight dots measured, the average separation between the neutral exciton and the additional finite-bias emission peak was (4.8 ± 0.6) meV, while the average separation of emission peaks originating from the *s* and *p* shells was (13 ± 3) meV. The main effect of changing the template width in these cases was to change the QD neutral exciton emission energy, as the QD lateral size accommodates to the width of the (100) top surface of the template and the corresponding dot height changes.[22,23]

B. Fine-structure splitting

To further exclude the possibility of charged excitons within the present experiments, we investigate a dot (QD2) in which the AES is observable at zero applied bias using higher spectral resolution. Photoluminescence data from QD2 as a function of the lateral electric field are shown in Fig. 5(a). At 0 V bias, transitions from the two neutral exciton states, split by eh exchange, are observed around 922.4 meV (1344 nm) with a separation of 108 μeV. The fine structure, or asymmetric exchange splitting (AES) of the two peaks as a function of electric field (bias), is shown in Fig. 5(b) (solid circles). With increasing bias, the AES diminishes, reaching a level of 56 μeV at 1.5 V. Beyond 1.5 V, the

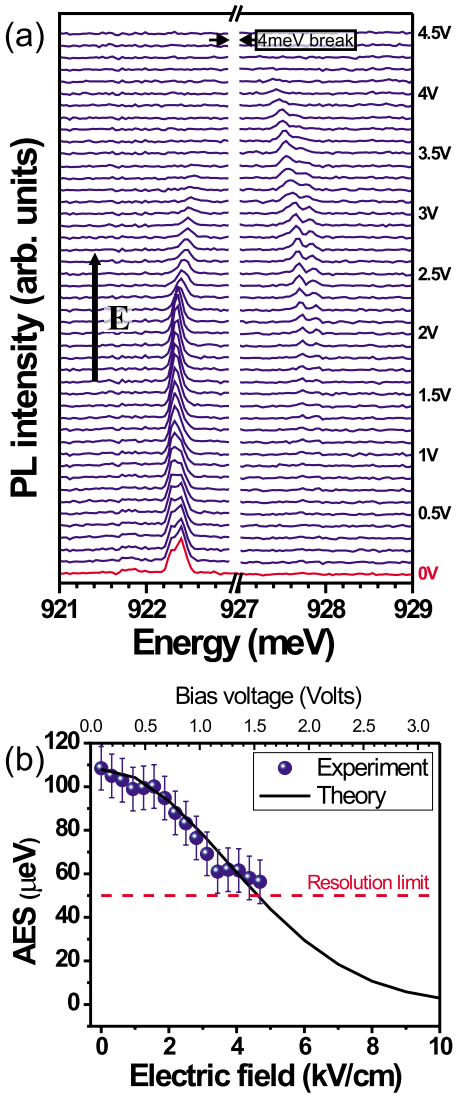

FIG. 5. (Color online) (a) Electric-field-dependent high-resolution PL spectra measured with a quantum dot exhibiting the anisotropic exchange splitting. (b) Analysis of fine-structure splitting (AES) from (a) as a function of lateral electric field. Excellent agreement between the measured (closed blue circles) and calculated AESs (solid black line) is obtained, thus, verifying our assignment of observed transitions.

AES is below the instrumental resolution (50 μeV—dotted red line) and the oscillator strength of the X decays monotonically. Both the value of the AES and its reduction with applied field are consistent with the behavior observed previously for single excitons confined in InAs/GaAs quantum dots by Kowalik *et al.*[20] In Fig. 5(b), we compare the calculated (solid black line) and measured (solid blue circles) fine-structure splittings as a function of lateral electric field. Details of our calculations are presented elsewhere.[10] Here let us only mention that the observed behavior is traced to the electric-field-induced separation of the electrons and holes, which decreases the magnitude of the electron-hole exchange elements responsible for AES. The result of the calculation is in excellent agreement with experiment, thus, confirming the assignment of the X transition in our data. The reduction in AES is expected due to the field-induced separation of carriers by the lateral electric field and the corresponding decrease in electron-hole overlap.[26]

In addition to the reduction in the AES and oscillator strengths of the ground-state transitions by the applied lateral field, the average of the emission energy for the two AES split peaks exhibits a small redshift with increasing bias. At approximately 1.9 V, a blue-shifting peak is observed at an energy of approximately 922.4 meV. We attributed this peak to the onset of biexciton emission corresponding to a situation in which the lifetime of the ground state X is increasing rapidly under applied field.[5] The blueshift of the biexciton is confirmed by a theoretical calculation,[10] suggesting that it is possible to obtain degeneracy between the biexciton and exciton transitions. The appearance of the blue-shifting transition is accompanied by a quenching of the ground-state transitions involving s-shell electrons and s-shell holes, with the simultaneous appearance of the s-p forbidden transition involving s-shell electrons and p-shell holes at ~5 meV higher energy. In the voltage range from approximately 1.5 to 4 V, we observe not one but two additional transitions around 927.5 meV. The splitting of ~200 μeV for these two peaks is larger than the expected AES at this field since the exchange splitting for the ground state X is already below the spectral resolution of the experiment (<50 μeV). The appearance of two features instead of the anticipated one can be explained by the dot asymmetry, leading to the misalignment of the hole p_x and p_y orbitals with respect to the direction of applied field. We note that the observed splitting for the higher-energy peak would not be present for the ground state of a charged exciton species in the singlet configuration but is fully explained with our interpretation involving a p-shell hole.

III. THEORETICAL MODEL

To understand the effects observed under applied lateral electric field, we model the QD by an isotropic two-dimensional harmonic-oscillator (HO) potential. A similar theoretical model was recently developed by Ritter *et al.*[27] For the electric field E applied along the x axis (i.e., along the ridge), the confining potential in the x direction, $V_e(x) = \frac{1}{2}m_e^*\omega_e^2x^2 - eEx$, remains parabolic. Here m_e^* and e are the effective mass and charge of the electron, respectively, and $\hbar\omega_e$ is the characteristic HO energy. The potential can be rewritten as $V_e(x) = \frac{1}{2}m_e^*\omega_e^2(x-\Delta x_e)^2 - \Delta\varepsilon_e$, with a displacement of the origin, $\Delta x_e = +eE/m_e^*\omega_e^2$, and the Stark shift, $\Delta\varepsilon_e = -(eE)^2/(2m_e^*\omega_e^2)$. For positively charged holes the confinement potential takes the form $V_h(x) = \frac{1}{2}m_h^*\omega_h^2(x-\Delta x_h)^2 - \Delta\varepsilon_h$ with the heavy-hole mass m_h^*, the hole HO energy $\hbar\omega_h$, the displacement $\Delta x_h = -eE/m_h^*\omega_h^2$, and the Stark shift $\Delta\varepsilon_h = -(eE)^2/(2m_h^*\omega_h^2)$. Here, the electric field shifts the origins of the electron and hole potentials in opposite directions, leading to a separation of carriers. The single-particle HO energies corresponding to the above confinement potentials are $\varepsilon_{nm}^{\beta} = \hbar\omega_\beta(n+m+1) - \Delta\varepsilon_\beta$, with quantum numbers $n, m = 0, 1, \ldots$ and the index $\beta = e, h$ identifying the carrier type. Both electrons and holes experience Stark shifts toward lower energies. However, the characteristic HO energies $\hbar\omega_\beta$

remain unchanged, which means that the intershell spacings and shell degeneracies do not depend on the electric field. Therefore, the single-particle wave functions, $|nm\rangle$, are simply the displaced two-dimensional HO orbitals.

The Hamiltonian of the interacting electrons and holes confined in the QD can be written as

$$H = \sum_i \varepsilon_i c_i^\dagger c_i + \sum_j \varepsilon_j h_j^\dagger h_j + \frac{1}{2}\sum_{ijkl} \langle ij|V_{\rm ee}|kl\rangle c_i^\dagger c_j^\dagger c_k c_l + \frac{1}{2}\sum_{ijkl} \langle ij|V_{\rm hh}|kl\rangle h_i^\dagger h_j^\dagger h_k h_l - \sum_{ijkl} \langle ij|V_{\rm eh}|kl\rangle c_i^\dagger h_j^\dagger h_k c_l, \quad (1)$$

where the composite indices $i=nm\sigma$ (likewise j,k,l) enumerate the electron and hole orbitals, σ denotes the carrier spin ($\pm 1/2$ for electrons and $\pm 3/2$ for holes), and c_i and $c_i^\dagger$ (h_i, $h_i^\dagger$) denote, respectively, the annihilation and creation operators for electrons (holes). In this Hamiltonian, the first two terms account for the single-particle properties, and the following three terms describe the electron-electron, hole-hole, and direct electron-hole Coulomb interactions, respectively. The matrix elements scaling these interactions are obtained by direct integration in the harmonic-oscillator basis.

Eigenenergies and eigenstates of the Hamiltonian (1) are calculated within a configuration-interaction approach. This involves creating all possible configurations of N_e electrons and N_h holes on the three lowest single-particle shells (s,p,d), forming the Hamiltonian matrix in the basis of these configurations and diagonalizing it numerically. Using the resulting excitonic eigenenergies and eigenvalues, we calculate the emission spectrum using Fermi's golden rule,

$$I(\omega) = \sum_f |\langle f, N_e - 1, N_h - 1|P^-|i, N_e, N_h\rangle|^2 \delta(E_i - E_f - \hbar\omega). \quad (2)$$

Here, P^- is the interband polarization operator removing one electron-hole pair from the system, $P^- = \Sigma_{ij}\alpha_{ij}c_i h_j$, and $\alpha_{ij} = {}_e\langle i|j\rangle_h$ is the overlap integral controlling the optical selection rules for the emission. In the calculations presented here we assume the following system parameters: $\hbar\omega_e = 12$ meV, $m_e^* = 0.055 m_0$, $\hbar\omega_h = 6$ meV, and $m_h^* = 0.11 m_0$ with m_0 being the mass of a free electron. In the following, we express energies in units of excitonic Rydberg (Ry), where Ry $= m_e^* e^4/2\varepsilon^2\hbar^2$. Here, ε is the dielectric constant of the material. With $\varepsilon = 12.4$, we have Ry $= 4.867$ meV for our system.

A. Exciton Stark shift

The lowest-energy state of a single electron-hole pair confined in the QD is well approximated by the configuration $|X_0\rangle = c_{(00\downarrow)}^\dagger h_{(00\uparrow)}^\dagger|0\rangle$, in which both carriers occupy the s-shell orbital. The energy of this state, $E_X = \varepsilon_e(00) + \varepsilon_h(00) - V_{\rm eh} - \Delta E_X^{\rm corr}$, consists of single-particle energies of the occupied orbitals (two first terms), the electron-hole interaction element $V_{\rm eh} = \langle 00,00|V_{\rm eh}|00,00\rangle$, and the correlation correction (last term) arising as a result of mixing of the configuration $|X_0\rangle$ with higher-lying exciton configurations. As already discussed, the single-particle energies of the electron and hole, $\varepsilon_e(00)$ and $\varepsilon_h(00)$, exhibit a Stark redshift quadratic in E. The sum of these two energies as a function of the field was used as the single-particle estimate of the Stark shift shown in Fig. 3. We replot it in Fig. 6(a) with a dotted blue line.

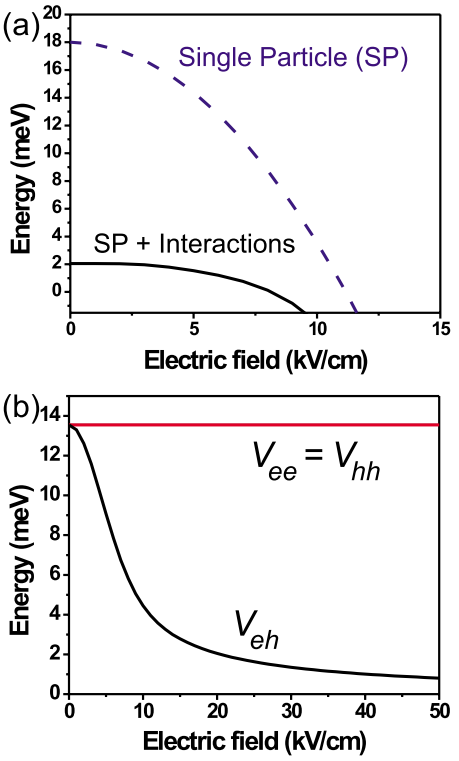

FIG. 6. (Color online) (a) Calculated exciton Stark shift without (blue dotted line) and with Coulomb electron-hole interactions (black solid line). (b) Fundamental Coulomb matrix element $V_{\rm ee}$, $V_{\rm hh}$, and $V_{\rm eh}$ calculated as a function of the electric field.

Let us now account for the Coulomb electron-hole interactions composing the exciton energy. In Fig. 6(b) we plot the fundamental matrix element $V_{\rm eh}$ as a function of the field together with the fundamental electron-electron ($V_{\rm ee}$) and hole-hole ($V_{\rm hh}$) elements. The electron-electron and hole-hole elements are independent of the field, since the symmetry or spatial extent of the HO orbitals do not change and the relative distances between carriers of the same type remain the same. In contrast, the electron-hole element $V_{\rm eh}$ decreases exponentially with the increase in the field due to the spatial separation of the charges. Since this element enters the exciton energy with the negative sign, it partially compensates for the single-particle redshift, as shown in Fig. 6(a) with the solid black line. The calculated polarizability β of this exciton is 30 μeV cm^2/kV^2; however, we find that it is sensitive to the confinement energies of the system. This is not surprising, since the effective Stark shift results from the interplay of single-particle effects and Coulomb interactions, and these depend sensitively on the confinement strength. The calculated polarizability is still larger than the one obtained experimentally ($\beta = 0.31$ μeV cm^2/kV^2), but this fundamental result qualitatively explains the strong reduction in the Stark shift as compared to the single-particle picture and accounts for the small energy shift observed in Fig. 2. A more accurate estimate of the expected polarizability requires a

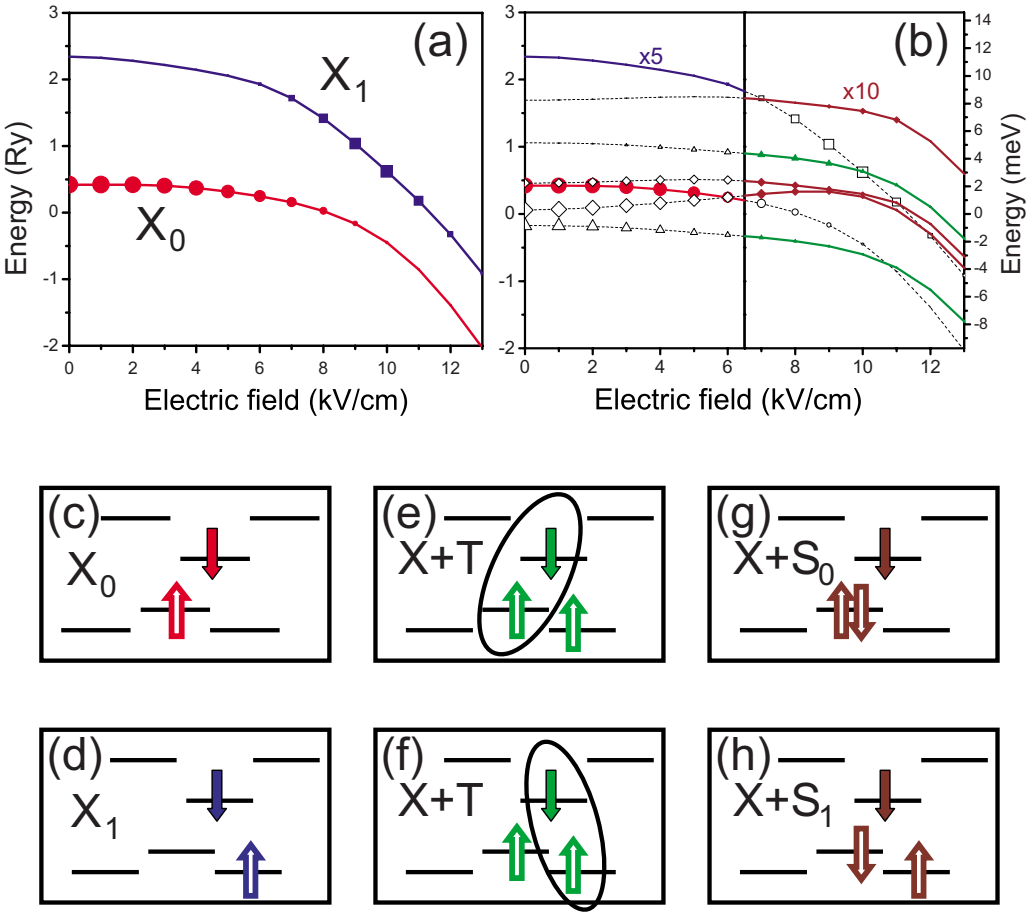

FIG. 7. (Color online) (a) Calculated emission spectra from the excitonic ground (X_0—red circles) and first excited states (X_1—blue squares) as a function of the electric field. (b) Calculated emission spectra of the neutral exciton and the positively charged exciton complex in the hole triplet (green triangles) and hole singlet (brown diamonds) configurations. The vertical line denotes the addition of an extra hole (see text for discussion). In both panels the size of the symbols is proportional to the calculated emission amplitude. Panels (c) and (d) show the ground, X_0, and excited states X_1 of the neutral exciton, respectively. Panels (e) and (f) show the ground-state configuration of the triplet charged exciton $X+T$; the carriers undergoing radiative recombination are marked with the oval. Panels (g) and (h) show the ground and first-excited configurations of the singlet charged exciton $X+S$ and $X+S_1$, respectively.

detailed understanding of the size and shape of the dot confinement, which is outside of the scope of the present analysis.

The above argument does not apply in vertical electric fields. Due to the small QD height (several nanometer) the electrons and holes cannot be efficiently separated, which results in a much weaker dependence of V_{eh} on the field. As a result, the Stark shift is dominated by the single-particle effect, which explains the good agreement between the estimated and measured exciton polarizabilities in such systems.

B. Transition at finite bias

The first excited exciton state, $|X_1\rangle = c^{\dagger}_{(00\downarrow)} h^{\dagger}_{(01\uparrow)} |0\rangle$, is formed by placing the electron on the *s*-shell orbital, but the hole is placed on one of the *p*-shell orbitals. At zero electric field such a state is dark due to the zero overlap between the electron and hole orbitals. At finite bias, however, radiative recombination from this state becomes allowed, resulting in the appearance of the additional maximum in the emission spectra. The calculated positions of emission peaks of the exciton in the ground, $|X_0\rangle$, and excited states $|X_1\rangle$ as a function of the field are plotted in Fig. 7(a), while the dominant configurations of the two exciton states are shown schematically in Figs. 7(c) and 7(d), respectively.

In Fig. 8 we compare the measured integrated intensity of the peaks observed in Fig. 5 and the calculated strength of the emission maxima as a function of lateral electric field for both excitonic states. To find the calibration between the experimental bias voltage ΔV and the electric field E used in calculations, we align the maximum intensity of the calculated and measured $|X_1\rangle$ peak. The calculated strength of transitions (solid lines) is in excellent agreement with the measured intensity (open symbols). The $|X_0\rangle$ transition intensity decreases monotonically with increasing electric field, while the $|X_1\rangle$ transition becomes allowed for finite fields.

To confirm the validity of our calibration procedure for the electric field, we calculate the electric field between the electrodes using the approach in Ref. 21. We assume that the electrodes are separated by a distance d and the dot is an infinite thin slab between the electrodes with a thickness much less than d. For such an approximation, we calculate

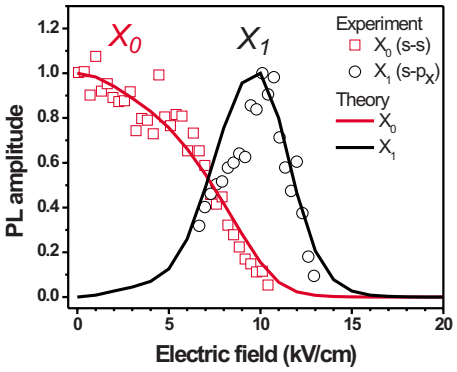

FIG. 8. (Color online) Measured (open symbols) and calculated (solid lines) emission intensities as a function of lateral electric field for the ground X_0 (red) and first excited X_1 (black) exciton states.

the electric field, E, applied across the QD as $E=\Delta V/\varepsilon d$. Here, $\varepsilon=12.4$ is the dielectric constant of InP. This simple scaling agrees with that used in Fig. 8 to within 7%.

IV. CHARGED EXCITON COMPLEXES

To further preclude the presence of charged exciton species for the transition appearing under applied bias, we have performed additional CI calculations corresponding to recombination events from both singlet and triplet singly charged excitons involving X^+ and X^-. Here we present a detailed discussion of the positively charged excitons only, since the behavior of the emission spectra of negatively charged excitons is qualitatively the same.

The spectra of the exciton and all positively charged exciton complexes as a function of the electric field are shown in Fig. 7(b). In this figure we assume that for small fields we deal only with a charge-neutral electron-hole pair. The corresponding positions of emission peaks in this region are plotted with solid lines, with the emission peaks from $|X_0\rangle$ ($|X_1\rangle$) denoted as red circles (blue squares). At the field of $E=6.5$ kV/cm we add an extra hole. In this region of the fields the emission spectra of the $|X+T\rangle$ complex are marked by green triangles while those of the $|X+S\rangle$ complex are marked by brown diamonds. The open symbols in the right (left) panel represent the continuation of the calculated uncharged (charged) spectra.

Let us now describe the spectra of charged excitons in greater detail. The positively charged exciton has two possible main configurations: with holes forming a spin-triplet $|X+T\rangle$ and a spin-singlet $|X+S\rangle$. We start with the $|X+T\rangle$ complex, whose ground state is well approximated by the lowest-energy configuration $|X+T\rangle=c^\dagger_{00\downarrow}h^\dagger_{00\uparrow}h^\dagger_{01\uparrow}|0\rangle$. This configuration is shown schematically in Figs. 7(e) and 7(f). The radiative recombination from this state can take place in two ways: (i) the s-shell electron recombines with the s-shell hole, as shown in Fig. 7(e), or (ii) the s-shell electron can recombine with the p-shell hole, as shown in Fig. 7(f). As a result, we expect two emission lines, with the case (ii) realized only at finite fields. In Fig. 7(b) we find these lines (green triangles) on either side of the $|X_0\rangle$ emission line (red circles). This is not observed in the experiment. Note that the lower line, arising from the case (i), corresponds to energies lower than $|X_0\rangle$, with the extra binding energy being due to additional correlations brought about by the presence of the extra hole. Also, the low-lying line exhibits a monotonic redshift. This is in contrast to the behavior observed in Fig. 5, where the $|X_0\rangle$ line is continued by a blue-shifting maximum and no lower-lying maxima are detected.

In the case of $|X+S\rangle$ we account for two configurations. In one of them both holes occupy the s shell, $|X+S_0\rangle=c^\dagger_{00\downarrow}h^\dagger_{00\uparrow}h^\dagger_{00\downarrow}|0\rangle$, as shown schematically in Fig. 7(g). In this case the radiative recombination involves only the carriers from the s shell. In the second configuration the holes occupy the s and p shells, $|X+S_1\rangle=(c^\dagger_{00\downarrow}h^\dagger_{00\uparrow}h^\dagger_{01\downarrow}|0\rangle+c^\dagger_{00\downarrow}h^\dagger_{01\uparrow}h^\dagger_{00\downarrow}|0\rangle)/\sqrt{2}$, as shown in Fig. 7(h). Here the emission can occur as a result of recombination of the s-shell electron and either s-shell or p-shell hole. The three emission lines corresponding to the $|X+S\rangle$ complex are shown in Fig. 7(b) with brown diamonds. The highest-energy $|X+S\rangle$ emission line appears to be a good candidate for the additional emission maximum seen in the experiment. However, its Stark shift is comparable to that of the neutral exciton in the $|X_0\rangle$ configuration (red circles), while the Stark shift of the neutral $|X_1\rangle$ configuration (blue squares) is much larger. The smaller Stark shift of the $|X+S\rangle$ line than $|X_1\rangle$ is due to the fact that the suppression of the electron-hole interactions is larger, as the electron interacts with two holes instead of only one. This same argument can be applied to all other charged complexes presented in Fig. 7(b).

We have performed a similar analysis for the negatively charged exciton X^-, which is composed of a single hole and two electrons (not shown in Fig. 7). We find that the position and behavior of emission maxima resulting from the recombination of the s-shell hole and the s-shell electron are very similar to the respective X^+ peaks. The recombination of the s-shell hole and the p-shell electron, on the other hand, results in the emission of a higher-energy photon compared to that in the X^+ complex because of the larger electron confinement energy. The field dependence of the X^- peaks, being qualitatively the same as that of the X^+ maxima, combined with the additional energy argument allows us to exclude the presence of the negatively charged exciton in the measured spectra.

In the eight dots studied, the measured Stark shift of the extra emission peak at higher energy was larger than that of the neutral exciton in all cases, thus, confirming our assignment of the s-p ($|X_1\rangle$) transition observed in the experiment. Moreover, due to the singlet character of the hole state, the $|X+S\rangle$ emission maxima in the ground state [configuration in Fig. 7(g)] are not expected to have any fine structure, while in the experiment the AES is detected for the low-energy peak. To conclude, the number, position, Stark shift, and fine structure of the emission peaks expected for the positively and negatively (data not shown) charged excitons do not match our experimental spectra, which allows us to exclude the presence of charged excitons appearing in a lateral electric field for our samples.

V. CONCLUSIONS

In conclusion, our results demonstrate a postgrowth tuning technique that allows one to electrically manipulate the

electronic properties of individual site-selected InAs/InP QDs. Photoluminescence data as a function of applied lateral electric field show an excitonic Stark Shift that is two orders of magnitude smaller than that expected from single-particle calculations. The polarizability of the ground-state transition (β=0.31 μeV cm^2/kV^2) is understood through the exponential decay of the electron-hole Coulomb interaction under applied lateral electric field. The observed modification of oscillator strengths for the excitonic transitions and the appearance of a normally forbidden excited state of the neutral exciton are in excellent agreement with our many-body configuration-interaction calculations of the emission spectra.

An ability to electrically switch between the ground-state and forbidden transitions is expected to find application in advanced single-photon sources or electron-spin resonance techniques, or as a quantum logic gate in all optical quantum computing,[28] while the Stark shift produced by the electric field can be utilized as a tuning method to improve the timing jitter of single-photon sources.[29] Finally, the scalable gating technology, which (in this work) is utilized to apply a lateral electric field to prepositioned InAs/InP QDs, allows the possibility for creating arrays of entangled photon pair sources on demand without the requirement to remove the fine-structure splitting, as proposed recently.[5,10]

ACKNOWLEDGMENTS

The authors acknowledge financial support from the Canadian Institute for Advanced Research, the Canadian Institute for Photonic Innovations, QuantumWorks, and the Natural Sciences and Engineering Research Council.

*michael.reimer@nrc.ca

[1] P. Hawrylak and M. Korkusinski, in *Single Quantum Dots: Fundamentals, Applications, and New Concepts*, Topics in Applied Physics Vol. 90, edited by P. Michler (Springer-Verlag, Berlin, 2003).
[2] J. Lefebvre, P. J. Poole, J. Fraser, G. C. Aers, D. Chithrani, and R. L. Williams, J. Cryst. Growth **234**, 391 (2002).
[3] S. Frédérick, D. Dalacu, J. Lapointe, P. J. Poole, G. C. Aers, and R. L. Williams, Appl. Phys. Lett. **89**, 091115 (2006).
[4] M. E. Reimer, W. R. McKinnon, J. Lapointe, D. Dalacu, P. J. Poole, G. C. Aers, D. Kim, M. Korkusinski, P. Hawrylak, and R. L. Williams, Physica E (Amsterdam) **40**, 1790 (2008).
[5] M. E. Reimer, M. Korkusinski, J. Lefebvre, J. Lapointe, P. J. Poole, G. C. Aers, D. Dalacu, W. R. McKinnon, S. Frederick, P. Hawrylak, and R. L. Williams, arXiv:0706.1075 (unpublished).
[6] N. Gisin and R. Thew, Nat. Photonics **1**, 165 (2007).
[7] N. Gisin, G. Ribordy, W. Tittel, and H. Zbinden, Rev. Mod. Phys. **74**, 145 (2002).
[8] A. J. Shields, Nat. Photonics **1**, 215 (2007).
[9] C. Santori, D. Fattal, J. Vuckovic, G. S. Solomon, and Y. Yamamoto, Nature (London) **419**, 594 (2002).
[10] M. Korkusinski, M. E. Reimer, R. L. Williams, and P. Hawrylak (unpublished).
[11] R. M. Stevenson, R. J. Young, P. Atkinson, K. Cooper, D. A. Ritchie, and A. J. Shields, Nature (London) **439**, 179 (2006).
[12] N. Akopian, N. H. Lindner, E. Poem, Y. Berlatzky, J. Avron, D. Gershoni, B. D. Gerardot, and P. M. Petroff, Phys. Rev. Lett. **96**, 130501 (2006).
[13] A. Greilich, M. Schwab, T. Berstermann, T. Auer, R. Oulton, D. R. Yakovlev, M. Bayer, V. Stavarache, D. Reuter, and A. Wieck, Phys. Rev. B **73**, 045323 (2006).
[14] B. D. Gerardot, S. Seidl, P. A. Dalgarno, R. J. Warburton, D. Granados, J. M. Garcia, K. Kowalik, O. Krebs, K. Karrai, A. Badolato, and P. M. Petroff, Appl. Phys. Lett. **90**, 041101 (2007).
[15] K. Kowalik, O. Krebs, A. Lemaitre, B. Eble, A. Kudelski, P. Voisin, S. Seidl, and J. A. Gaj, Appl. Phys. Lett. **91**, 183104 (2007).
[16] M. M. Vogel, S. M. Ulrich, R. Hafenbrak, P. Michler, L. Wang, A. Rastelli, and O. G. Schmidt, Appl. Phys. Lett. **91**, 051904 (2007).
[17] H. Drexler, D. Leonard, W. Hansen, J. P. Kotthaus, and P. M. Petroff, Phys. Rev. Lett. **73**, 2252 (1994).
[18] S. Raymond, J. P. Reynolds, J. L. Merz, S. Fafard, Y. Feng, and S. Charbonneau, Phys. Rev. B **58**, R13415 (1998).
[19] P. W. Fry, I. E. Itskevich, D. J. Mowbray, M. S. Skolnick, J. J. Finley, J. A. Barker, E. P. O'Reilly, L. R. Wilson, I. A. Larkin, P. A. Maksym, M. Hopkinson, M. Al-Khafaji, J. P. R. David, A. G. Cullis, G. Hill, and J. C. Clark, Phys. Rev. Lett. **84**, 733 (2000).
[20] K. Kowalik, O. Krebs, A. Lemaitre, S. Laurent, P. Senellart, P. Voisin, and J. A. Gaj, Appl. Phys. Lett. **86**, 041907 (2005).
[21] J. Seufert, M. Obert, M. Scheibner, N. A. Gippius, G. Bacher, A. Forchel, T. Passow, K. Leonardi, and D. Hommel, Appl. Phys. Lett. **79**, 1033 (2001).
[22] D. Chithrani, R. L. Williams, J. Lefebvre, P. J. Poole, and G. C. Aers, Appl. Phys. Lett. **84**, 978 (2004).
[23] W. Sheng and P. Hawrylak, Phys. Rev. B **72**, 035326 (2005).
[24] F. Findeis, M. Baier, E. Beham, A. Zrenner, and G. Abstreiter, Appl. Phys. Lett. **78**, 2958 (2001).
[25] E. S. Moskalenko, M. Larsson, W. V. Schoenfeld, P. M. Petroff, and P. O. Holtz, Phys. Rev. B **73**, 155336 (2006).
[26] M. Bayer, G. Ortner, O. Stern, A. Kuther, A. A. Gorbunov, A. Forchel, P. Hawrylak, S. Fafard, K. Hinzer, T. L. Reinecke, S. N. Walck, J. P. Reithmaier, F. Klopf, and F. Schäfer, Phys. Rev. B **65**, 195315 (2002).
[27] S. Ritter, P. Gartner, N. Baer, and F. Jahnke, Phys. Rev. B **76**, 165302 (2007).
[28] A. D. Greentree, J. Salzman, S. Prawer, and L. C. L. Hollenberg, Phys. Rev. A **73**, 013818 (2006).
[29] M. J. Fernée, H. Rubinsztein-Dunlop, and G. J. Milburn, Phys. Rev. A **75**, 043815 (2007).